THE GREENLAND FLOW DISTORTION EXPERIMENT

BY I. A. RENFREW, G. W. K. MOORE, J. E. KRISTJÁNSSON, H. ÓLAFSSON, S. L. GRAY, G. N. PETERSEN, K. BOVIS, P. R. A. BROWN, I. FØRE, T. HAINE, C. HAY, E. A. IRVINE, A. LAWRENCE, T. OHIGASHI, S. OUTTEN, R. S. PICKART, M. SHAPIRO, D. SPROSON, R. SWINBANK, A. WOOLLEY, AND S. ZHANG

We present an overview of an aircraft-based field campaign focusing on the dynamics and air–sea interaction associated with tip jets, barrier winds, and mesoscale cyclones, as well as a targeted observation program.

A millennium ago pioneering Icelanders and Norwegians were exploring and settling the southern coastline of Greenland when, almost accidentally, they stumbled across North America. Their exploits are recorded in the *Icelandic Sagas*,[1] some of the oldest writing in the western world, including the *Vinland Sagas*, which contain two largely consistent accounts of these events. In both of these narratives, stormy weather plays a pivotal role. In *Eirik the Red's Saga* Eirik's son, Leif Eiriksson, departs for Greenland, whereupon

> **After being tossed about at sea for a long time he chanced upon land where he had not expected any to be found. Fields of self-sown wheat and vines were growing there; also, there were trees known as maple.**

In *The Sagas of the Greenlanders*, Bjarni Herjolfsson is blown off course, ▶

[1] The *Icelandic Sagas* are derived from the oral tradition of recounting historical events and so tend to have been written down (often anonymously) many years after the events they describe. The translations quoted here are from the compendium *The Sagas of the Icelanders: A Selection*, Preface—J. Smiley, Introduction—R. Kellogg, published by Penguin Books, 2000; with these translations first published in *The Complete Sagas of Icelanders*, Volumes I-V, Leifur Eiríksson Publishing Ltd, Iceland, 1997. A recent review of environmental understanding amongst the early Norse cultures can be found in the article by Haine (2008).

Coastal mountains of southeast Greenland, at about 66°N, 35°W, on 5 March 2007. (Photo: G.W.K. Moore)

"beset by winds from the north and fog," journeying from Iceland to Greenland; while lost to the west of Greenland, he sighted "land that was not mountains but did have small hills and was covered with forests." On finally arriving in Greenland, Bjarni describes these new lands to Eirik the Red, whereupon Leif Eiriksson purchases Bjarni's ship and sets sail for this new "Vinland." In both *Vinland Sagas*, fierce winds in the vicinity of southern Greenland are instrumental in this first discovery and initial exploration by Europeans of what was to become North America. Now, a millennium later, fierce winds off southern Greenland are again thought to be highly influential; however, this time these winds influence the climate system, not explorers.

Greenland's presence in the central North Atlantic provides a massive topographic barrier at the northern fringes of the primary synoptic-scale midlatitude storm track. Interactions between the synoptic-scale flow and this barrier are known to generate a myriad of mesoscale weather systems, many of which have only been observed relatively recently via satellite or numerical modeling simulations. For example, while undertaking a numerical modeling study of gravity wave generation over Greenland, Doyle and Shapiro (1999) made the fortuitous discovery of a high wind speed westerly "tip jet" emanating from Cape Farewell, at the southern point of Greenland (Fig. 1). They proposed that the jet was caused by acceleration down the lee slope, under conservation of the Bernoulli function, and by flow distortion around the cape. A series of idealized modeling studies of flow impinging on large barriers has also shown similar tip jets resulting from flow distortion acclerations (Ólafsson and Bougeault 1996, 1997; Petersen et al. 2003, 2005; Orr et al. 2005; Egger 2006). Numerical weather prediction (NWP) modeling studies both with and without Greenland's high mountains have

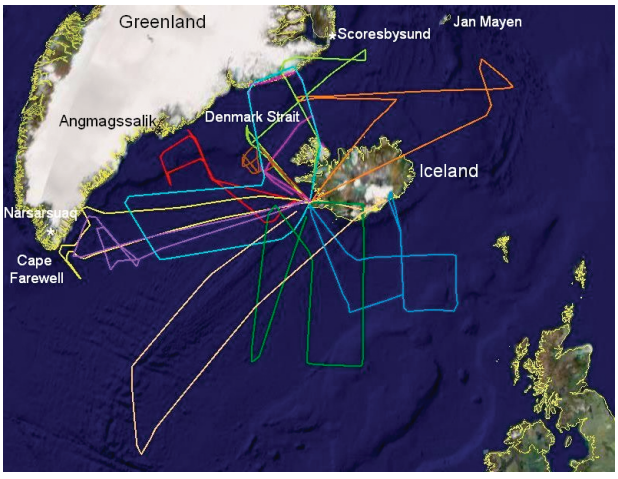

Fig. 1. Flight tracks of the FAAM during the GFDex campaign. The detachment base was Keflavik Airport in Iceland. Flight tracks are as follows: B268, yellow; B269, missing; B270, dark green; B271, orange; B272, blue; B273, cyan; B274, magenta; B275, violet; B276, red; B277, light green; B278, brown; and B279 beige. See Table 1 for flight plan descriptions. Selected radiosonde stations and other relevant locations are indicated.

shown its importance in generating lee cyclones, developing transient cyclones, and developing polar mesoscale cyclones (Kristjánsson and McInnes 1999; Schwierz and Davies 2003; Skeie et al. 2006; Klein and Heinemann 2002). Indeed, polar mesocyclone satellite- and reanalysis-based climatologies have shown the lee of southeast Greenland to be highly populated with mesoscale cyclones (Harold et al. 1999; Condron et al. 2006). Furthermore, the large-scale slopes and high-latitude location of Greenland means it is also prone to density-driven katabatic flows, locally known as *piteraqs,* which can often reach the coast (see, e.g., Heinemann 1999; Cappelen et al. 2001) and can lead to cyclogenesis (Klein and Heinemann 2002).

AFFILIATIONS: Renfrew, Petersen, Outten, and Sproson—School of Environmental Sciences, University of East Anglia, Norwich, United Kingdom; Moore, Hay, Ohigashi, and Zhang,—Department of Physics, University of Toronto, Toronto, Ontario, Canada; Kristjánsson and Føre—Department of Geophysics, University of Oslo, Oslo, Norway; Ólafsson—Department of Physics, University of Iceland, Reykjavik, Iceland, and University of Bergen, Bergen, Norway; Gray and Irvine—Department of Meteorology, University of Reading, Reading, United Kingdom; Bovis, Brown, and Swinbank—Met Office, Exeter, United Kingdom; Haine—Department of Earth and Planetary Sciences, Johns Hopkins University, Baltimore, Maryland; Lawrence—European Centre for Medium-Range Weather Forecasts, Reading, United Kingdom; Pickart—Department of Physical Oceanography, Woods Hole Oceanographic Institution, Woods Hole, Massachusetts; Shapiro—NOAA/Environmental Technology Laboratory, Boulder, Colorado; Woolley—Facility for Airborne Atmospheric Measurement, Cranfield, United Kingdom
CORRESPONDING AUTHOR: I. A. Renfrew, School of Environmental Sciences, University of East Anglia, Norwich, NR4 7TJ, United Kingdom
E-mail: i.renfrew@bas.ac.uk

The abstract for this article can be found in this issue, following the table of contents.
DOI:10.1175/2008BAMS2508.1

In final form 29 February 2008

Several recent climatologies of the Greenland area, using station observations (Cappelen et al. 2001), National Centers for Environmental Prediction (NCEP) reanalysis (Moore 2003), and Quick Scatterometer (QuikSCAT) satellite-derived winds (Moore and Renfrew 2005), have picked out and categorized several well-defined flow distortion features, namely, westerly tip jets and easterly reverse tip jets off Cape Farewell, and barrier winds off the southeast Greenland coast in the southern and northern Denmark Strait (Fig. 1). Moore and Renfrew (2005) hypothesize that these barrier winds are in thermal wind balance and are caused by cold (dense) synoptically driven flow being "piled up" against the high topography of southeast Greenland, in a similar manner to the barrier flows described in, for example, Schwerdtfeger (1975) and Parish (1982, 1983). This is in contrast to the thermally driven summertime barrier flows found on the western side of Greenland (van den Broeke and Gallee 1996). Moore and Renfrew (2005) also hypothesize that (easterly) reverse tip jets are barrier flows, which, as they reach Cape Farewell, undergo an easterly acceleration as they change from a thermal wind balance to an anticyclonic gradient wind balance.

In short, through distortion of the synoptic-scale flow, the topographic barrier of Greenland generates a myriad of mesoscale weather systems over the adjoining coastal seas. The high winds associated with these weather systems are a maritime hazard and, it has been suggested, have a profound impact on the ocean. For example, Doyle and Shapiro (1999) noted that the high heat fluxes associated with westerly tip jets could potentially play a role in the ocean's thermohaline circulation. Pickart et al. (2003) elaborated on this idea by suggesting that westerly tip jets trigger oceanic deep convection in the Irminger Sea (Fig. 1), demonstrating this possibility with idealized ocean modeling simulations. Våge et al. (2008) argue that the air–sea interaction associated with westerly tip jets is crucial to an explanation of the observed deepening of the oceanic mixed layer in the Irminger Sea. Moore and Renfrew (2005) speculate that reverse tip jets may influence the recirculation features in the southeast Labrador Sea described in Lavender et al. (2000) and Spall and Pickart (2003). Martin and Moore (2008) and Pickart et al. (2008) extend this idea to suggest that easterly reverse tip jets may play a role in forcing open-ocean convection in the secondary convection site that is associated with this recirculation feature, although this is called into question by Sproson et al. (2008). Moore and Renfrew (2005) also speculate that barrier flows play a role in preconditioning the Irminger Sea and in forcing oceanic jets within the East Greenland Current system (Bacon et al. 2002; Pickart et al. 2005), an idea also suggested by Pickart et al. (2005). Related to the above are some recent ocean modeling simulations, which suggest that (normally unresolved) mesoscale cyclones have a significant impact on water mass modification processes in the Nordic Seas, for example, enhancing mixed layer depths and Greenland Sea Deep Water overflow rates (Condron et al. 2008).

In addition to these local flow distortion features, it is known from numerical modeling studies that Greenland plays a role in the general circulation of the Northern Hemisphere through large-scale blocking (Schwierz and Davies 2003; Petersen et al. 2004), wave breaking (Doyle et al. 2005), and possibly triggering or guiding planetary-scale Rossby waves (Shapiro et al. 2002). Indeed, being a large barrier upstream of Europe, flow distortion due to Greenland affects synoptic-scale downstream development, and, thus, short- to medium-range atmospheric predictability and forecasting (e.g., Ólafsson 1998); to what extent this is the case is uncertain. To investigate such atmospheric predictability issues, a *targeted observation* program can be of use. The concept of targeting additional observations into areas of flow sensitivity (i.e., areas of rapid error growth in ensemble predicition systems) is an active area of research, particularly within the operational forecasting world (e.g., Montani et al. 1999; Langland et al. 1999; Szunyogh et al. 2000; Petersen and Thorpe 2007) and under the auspicises of the World Meteorological Organization's (WMO's) The Observing System Research and Predictability Experiment (THORPEX) program (Shapiro and Thorpe 2004). Prior to the recent Atlantic THORPEX Regional Campaign of 2003 an investigation of where analysis improvements would have led to 48-h forecast improvement for northern Europe indicated that a large area of the central North Atlantic was ideal, i.e., to the south of Iceland and Greenland (Stringer and Truscott 2004); and indeed during this 2003 campaign an aircraft was based in Iceland (Weissman et al. 2005).

Reviewing the above background provides ample motivation for a focused project to investigate both local and remote flow distortion effects due to Greenland. Being initiated in the run up to the International Polar Year (IPY) was fortuitous because the IPY facilitated a network of international project partners, as well as cooperation and funding from European Union (EU) national meteorological agencies. To summarize, the objectives of the Greenland Flow Distortion Experiment (GFDex) are to

- improve our understanding and ability to predict interactions between the atmospheric circulation and the topography of Greenland, both locally and downstream over Europe;
- obtain hitherto rare in situ observations of high-impact weather systems (e.g., tip jets, barrier winds, and polar mesoscale cyclones) and their associated air–sea fluxes in the coastal seas of Greenland;
- improve the numerical modeling of these weather systems, testing, for example, the boundary layer and turbulence parameterizations, and thus improving the quality of the atmospheric forcing fields that are essential for accurate atmosphere–ocean coupling; and
- increase knowledge of the sensitivity of the large-scale downstream flow to flow distortion caused by Greenland and investigate the predictability of weather systems over Europe through the use of targeted observations upstream in sensitive areas of the flow.

This paper provides an overview an of the GFDex observational program, which was primarily an aircraft-based field campaign during February and March 2007, at the dawn of the IPY.

GFDEX LOGISTICS. The GFDex's main observational platform was the Facility for Airborne Atmospheric Measurements (FAAM) aircraft (see the sidebar on the "The Facility for Airborne Atmospheric Measurements") based out of Keflavik, Iceland, during a 3-week period in February–March 2007. However, as a contribution to the IPY, additional radiosonde releases were carried out at a number of nearby stations (Fig. 1), namely, Keflavik (WMO station 04018) for all 3 weeks; Narsarsuaq (04270), Scoresbysund (04339), and Angmagssalik (04360) on Greenland, "on demand"; on the Norwegian island of Jan Mayen (01001) for 1 day; and from all vessels on the EU-Automated Shipboard Aerological Programme (E-ASAP) when in our area of operations (50°–70°N, 60°–10°W).

THE FACILITY FOR AIRBORNE ATMOSPHERIC MEASUREMENTS

The FAAM maintains the United Kingdom's new large-scale research aircraft, operational since 2004, replacing the Met Office's veteran C130. The FAAM aircraft is a modified BAe146, a midsized four-engine passenger jet, fitted with additional fuel tanks to extend its range to approximately 1,800 nm or over 6 h. It is flexible, with a minimum operating altitude down to 100 ft over the sea, and has the ability to profile down to 50 ft and up to a ceiling of about 35,000 ft. Its standard "science speed" is 200-kt indicated airspeed (~100 m s^{-1}). Operating under the Civil Aviation Authority (CAA) legislation it requires two pilots, two cabin crew members, and can accommodate up to 18 scientists.

Table SB1 lists the FAAM aircraft's "core" instrumentation. In addition to this, many campaigns also fit a specified selection of specialized radiometric instruments, additional cloud physics instruments, or an array of delicate chemistry instruments (e.g., see Fehsenfeld et al. 2006). Of course, there are both payload and power limits to any instruments fits. During GFDex we were primarily interested in dynamical and physical processes that were often some distance from our detachment base, so a "stripped down" aircraft fit was used, with just the core instrumentation listed in Table SB1. This was the FAAM aircraft's lightest science fit since commissioning and enabled us to break its endurance record 3 times during the campaign.

Prior to the GFDex detachment a self-calibration flight for the turbulence probe, one of our key instruments, was carried out. The flight was into a region of uniform horizontal wind and expected zero vertical velocity. The flight pattern consisted of i) pairs of straight and level runs on opposite headings, which are used to calculate a factor for the true airspeed calibrations; and ii) yawing (side to side) oscillations during turns to check the angles of attack and sideslip (the flow angles relative to the aircraft in its own vertical and horizontal planes) measurements and the offset angles of the Inertial Navigation Unit (INU) relative to the aircraft axes in the pitch (nose up/down) and roll (wings up/down) planes. Errors in all four of these parameters can contribute erroneous vertical wind signals that are correlated with the manouevres. The data from ii were processed using a scheme that minimizes vertical wind variance (A. R. Rodi 2007; personal communication). The correction factors were then applied when processing the final output datasets. The results suggest that, on average, the horizontal wind measurement uncertainities will be 0.27 m s^{-1}.

Table SB1. FAAM BAe-146 "core" instrumentation. (Further details on all instruments can be found at www.faam.ac.uk.)

Name	Instrument	Measures	Sampling rate
AVAPS	Airborne Vertical Atmospheric Profiler System (Vaisala RD93 GPS dropsondes)	Profiles of position, pressure, temperature, relative humidity, wind speed, and direction	2 Hz
BBR	Broadband radiometers (Pyranometers and pyrgeometers)	0.3–3-μm hemispheric irradiance, 0.7–3-μm hemispheric irradiance, 4–50-μm hemispheric irradiance	1 Hz
FFSSP	Fast Forward Scattering Spectrometer Probe (PMS canister instrument)	1-s-averaged values of droplet number concentration, liquid water content, mean volume radius, effective radius, and droplet size spectrum (1–50 μm)	1 Hz
PCASP	Aerosol size spectrum optical probe (PMS canister instrument)	1-s-averaged values of aearosol particle number concentration, mean volume radius, and size spectrum (0.1–3 μm)	1 Hz
2D-C	Two-dimensional cloud particle imaging probe (PMS canister instrument)	5-s-averaged values of particle number concentration, condensed water content, mean volume radius, precipitation rate, and size spectrum (25–800 μm)	1 Hz
2D-P	Two-dimensional precipitation particle imaging probe (PMS canister instrument)	5-s-averaged values of particle number concentration, condensed water content, mean volume radius, precipitation rate, and size spectrum (200–6,400 μm)	1 Hz
CO	AL5002 carbon monoxide	Carbon monoxide (CO), integration time is 1 s	1 Hz
CPC	TSI 3025A condensation particle counter	Condensation particles	1 Hz
General Eastern	Hygrometer (using the chilled-mirror technique)	Water vapor (dewpoint temperature) over range 220–320 K; note the instrument response time for dewpoints at the lower end of the measurement range can be up to 30 s; the overall measurement uncertainty is estimated to be ±0.25 K above 273.15 K, increasing to around ±1 K at 210 K	4 Hz
GPS	Patch	Aircraft position, velocity, and time standard	1 Hz
Heimann	Downward-facing radiometer	Brightness temperature (8–14 μm)	4 Hz
INU	Inertial navigation unit	Aircraft velocity components, attitude, attitude rates, ground speed, and drift angle (position and acceleration at 1 Hz)	32 Hz
Johnson Williams	Liquid water content probe	Concentration of liquid water in clouds using a heated wire resistance bridge over range 0–3 g m^{-3}; typical measurement uncertainity ±10%	4 Hz
Nephelometer	Integrating nephelometer (Rosemount pair inlet instrument)	Total scattering and hemispheric backscattering coefficient at three visible wavelengths (450, 550, and 700 nm)	1 Hz
Nevzorov	Liquid and total water content probe	Liquid and total (ice plus liquid) water in clouds using a heated wire over range 0.003–3 g m^{-1}; accuracy ±10%	8 Hz
NOx	TECO 42 chemiluminescence instrument	NO, NO_2, and NO_X; integration time is 10 s	1 Hz
Ozone	TECO 49 UV photometric instrument	Ozone (O_3); integration time is 4 s	1 Hz
RadAlt	Radar altimeter	Altitude (accuracy ±2%)	2 Hz
RVSM	Reduced vertical separation minimum data system	Static and pitot-static pressures, pressure altitude, and indicated air speed	32 Hz
Rosemount	Temperature sensors	Temperatures (deiced and nondeiced), calibrated over range −60° to 30°C; overall measurement uncertainty ±0.3°C	32 Hz
TWC	Total water content using a Lyman-alpha absorption hygrometer	Water (H_2O) over range 0–20 g kg^{-1} and accuracy ±0.15 g kg^{-1}	64 Hz
Turbulence probe	Turbulence (see also RVSM)	Air speed and incidence angle; three-dimensional wind components; overall measurement uncertainty ±0.2 m s^{-1}; see sidebar text	32 Hz
Video cameras	Upward, downward, forward, and rear-view cameras	Video recordings onto video-8 tapes	

A successful aircraft-based field program aimed at observing specific weather-system targets must have accurate and timely forecast products in order to make day-to-day flight planning decisions (Renfrew et al. 1999). During the GFDex we had a number of tailored forecast and sensitive area prediction (SAP) products available to us (see "The target observations program"). These included diagnostics from global

Table 1. Campaign summary. All times are UTC. SAP = Sensitive area prediction. The flight tracks are illustrated in Fig. 1.

Date	Flight	Science aim	Flight plan	Takeoff (UTC)	Landing (UTC)	Dropsondes
21 Feb	B268	Reverse tip jet at Cape Farewell	Three dropsonde legs across, along, and across jet; profile descent, then two 100-ft legs across jet	1048	1627	12
22 Feb	B269	Iceland wakes; flow distortion effects to south and east of Iceland	Low-level legs across wake at 500–2,000 ft; dropsondes released north of Iceland	1030	1432	2
24 Feb	B270	Targeted observations of a SAP, south of Iceland	High-level lawnmower pattern, dropsondes every 120 nm	0855	1445	11
25 Feb	B271	Polar low; long-lived mesoscale low in the vicinity of Jan Mayen	Two dropsonde legs crossing low; profile descent over sea ice; then 300-km-long low-level run at 100 ft	1035	1625	16
26 Feb	B272	Targeted observations of a SAP and a weak mesoscale cyclone, southeast of Iceland	Two dropsonde legs crossing low and covering SAP grid; one 2,000-ft leg through low	0855	1423	14
1 Mar	B273	Targeted observations of a SAP; lee cyclogenesis and a barrier wind to the west and northwest of Iceland	Four high-level dropsonde legs; 1–2 covering lee cyclogenesis area, 3–4 across barrier wind	0855	1356	18
2 Mar	B274	Barrier wind northwest of Iceland, in the Denmark Strait	Two dropsonde legs (repeat of legs 3–4 of B273); profile descent over northeast Iceland; then 300-km-long 100-ft leg down jet (modified in flight due to icing)	1107	1455	9
3 Mar	B275	Lee cyclone to the southeast of Greenland	Two dropsonde legs crossing low; profile descent, then two 5,000-ft legs crossing low center	0939	1536	16
5 Mar	B276	Barrier wind, south of the Denmark Strait	Low-level transit; six 100-ft legs across jet and over sea ice, one 2,000-ft leg across jet; one dropsonde leg across jet	1120	1706	8
6 Mar	B277	Barrier wind, in the Denmark Strait	Low-level legs at 100–500 ft across and along jet; profile ascent, then two dropsonde legs across jet	1027	1600	17
9 Mar	B278	Lagrangian surface fluxes west of Iceland, in the Denmark Strait	Low-level transit; four 100-ft legs, then two stacks of legs at 100, 1,500, and 2,500 ft following air parcel between stacks; profile ascent then dropsonde leg into the wind	1031	1511	6
10 Mar	B279	Targeted observations of a SAP in the central North Atlantic	High-level legs across developing cyclone with dropsondes every 120 nm; additional dropsonde over breaking mountain wave at Hvannadalshnjúkur, Iceland	0800	1400	15

models run by the Met Office and the European Centre for Medium-Range Weather Forecasts (ECMWF), plus diagnostics from the regional North Atlantic–European (NAE) model of the Met Office, High-Resolution Limited-Area Model (HIRLAM) output from the Icelandic Met Service, the fifth-generation Pennsylvania State University (PSU)–National Center for Atmospheric Research (NCAR) Mesoscale Model (MM5) run by Storm Weather Centre (Norway), as well as more focused MM5 runs from the University of Toronto over Greenland and from the University of Iceland over Iceland. A number of specified fields were available to us as graphics images, all of which were replotted to focus on our area of interest. We also had real-time Advanced Very High Resolution Radiometer (AVHRR) and Moderate Resolution Imaging Spectroradiometer (MODIS) satellite imagery automatically processed into image files covering our area of interest by the Dundee Satellite Receiving Station.

Operating out of Iceland provided some demanding flight-planning requirements because much of our area of interest was part of the trans-Atlantic "airway" for commercial air traffic. This meant we had to have an efficient daily flight-planning and decision-making timeline in order to get our airspace requirements approved. Typically take-off times were around 0900–1100 UTC (also local). Thus, with airspace notifications of about 24 h required, this meant early morning was the key time for flight planning. For this we relied heavily on our operational regional forecast products because these were typically available 3–4 h after analysis times, for example, at 0400 and 1600 UTC. In contrast, the University of Toronto MM5 forecasts were not used as the primary planning tool, because these were available too late (about 9 h after analysis time); instead, these were used to aid minor adjustments or provide additional diagnostics. Flexibility from air traffic control, cajoling by our aircraft operators, and early mornings from everyone involved ensured that, in general, our flight plans were realized.

WEATHER SYSTEMS PROGRAM. *Campaign overview.* During the GFDex detachment the FAAM's BAe-146 flew 67 science hours over 12 flights and released 144 dropsondes. The flight tracks are illustrated in Fig. 1 and summarized in Table 1. There were eight missions exclusively aimed at weather system targets and four missions aimed at targeting observations into SAPs, although three of these four also had weather system objectives. Most of the weather system flights comprised a high-level component, releasing dropsondes across the feature of interest, and a low-level component in the atmospheric boundary layer (ABL), measuring turbulent fluxes, etc. Problems with severe icing (see the "Icing" sidebar) during a descent in flight B274, about halfway through the campaign, led to us adjusting some of our later flight plans. In order to prevent key instruments

ICING

Severe icing accumulation on any aircraft can be a serious safety concern (e.g., Marwitz et al. 1997), while for instrumented aircraft any icing can cause instrument malfunction. During GFDex icing conditions were prevalent—we were often flying in clouds with supercooled water droplets and below-freezing air temperatures—and moderate icing occurred on four flights (B274, B276, B277, B278). A buildup of ~1 cm of ice on instruments attached to the port underwiring pylon during flight B276 on 5 March 2007 is shown. The lower inboard position contains an empty Particle Measuring System (PMS) canister while the (just visible) lower outboard position contains the small ice detector Mk1 with its forward-facing intake tube. Icing tended to occur during descents or ascents through cloud. The BAe-146's five-hole turbulence probe on the nose of the aircraft was particularly susceptible to icing. When this occurred, the high-resolution 3D wind components are not accurate. Instead, an alternative horizontal wind product was derived. This still uses the aircraft's INU to provide horizontal velocities, but takes airspeed information from the pilots' instruments rather than the turbulence probe. It also assumes that the angle of sideslip is zero and the angle of attack is equivalent to the INU pitch angle; that is, there is no relative updraft/downdraft. These assumptions generally hold satisfactorily for time scales of a second or more, and tests in icing-free regions suggest that horizontal wind components over such scales can be obtained with a relative accuracy of about 1 m s^{-1}.

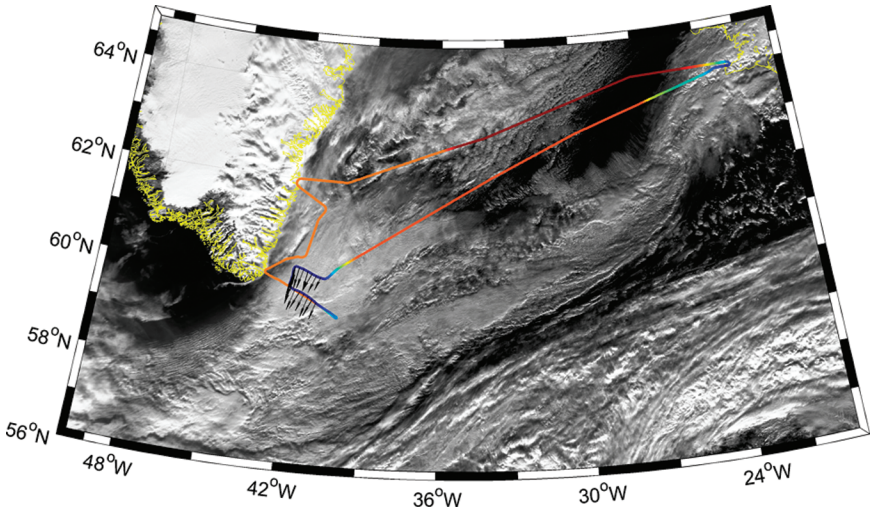

Fig. 2. Reverse tip jet flight track (B268) overlaid on a visible (channel 1) AVHRR satellite image from 1435 UTC 21 Feb 2007. The colors in the flight track indicate the aircraft's altitude from low (blue, ~30 m) to high levels (red, ~7,500 m). Wind vectors during the low-level legs are plotted every 100 s; these are typically 30–35 m s^{-1} in magnitude.

from icing up in cloud, we planned flights B276–B278 with a low-level transit and the low-level legs first. This worked well, but did mean substantial periods of time were spent at low levels, which was tiring for both the pilots and scientists and used additional fuel. To give a sense of the GFDex campaign, in the rest of this section we provide brief descriptions of several of the weather system missions. The results presented here are preliminary, but give an idea of the exciting observations gathered during the experiment.

A reverse tip jet. On 21 February 2007 there was a synoptic-scale barotropic low pressure system in the central North Atlantic at about 50°–55°N (not shown). Broad easterly flow was forecast to extend from 55° to 70°N in the longitudes between Iceland and Greenland, with the flow forecast to turn into a northeasterly barrier flow at low levels in the vicinity of Greenland. Our regional models forecast an acceleration of this barrier flow into a 30 m s^{-1} reverse tip jet curving around Cape Farewell. Associated with the strong winds were forecast surface sensible and latent heat fluxes of 140 and 200 W m^{-2}, respectively; despite the very strong winds, the air temperatures were not very cold, keeping the surface fluxes only moderate.

Figure 2 shows a visible satellite image from 1435 UTC 21 February 2007 with the flight track from B268 overlaid. The primary cloud shield associated with the synoptic-scale low dominated the southeast part of Fig. 2. Stretching to the southwest from Iceland is an elongated band of cloud. This is associated with an occluded front in the Met Office 1200 UTC analysis. Ahead of this there are mid- and low-level clouds to the southeast of Cape Farewell associated with the reverse tip jet. Note the cloud is densest slightly off the coast, indeed, there is a clearer slot running southwest–northeast from Cape Farewell. To the south there are well-defined cloud streets curving anticyclonically and delineating the northeast–east-northeast transition of the reverse tip jet. At Cape Farewell itself there is a thin streamer of cloud, which also curves anticyclonically into the clear air to the southwest of Greenland. The acceleration and curvature associated with this case is also clear in the scatterometer-derived near-surface winds (Fig. 3); according to QuikSCAT, the 25 m s^{-1} barrier winds accelerate to 40 m s^{-1} tip jet winds.

Our observations, the first aircraft-based observations of a tip jet feature, confirm these characteristics. The flight plan consisted of high-level dropsonde legs across, down, and back across the reverse tip jet; then a profile descent (turning halfway) completed the low-level legs across, into, and back across the jet at a minimum safe altitude (in this case ~30 m; see Fig. 2). The

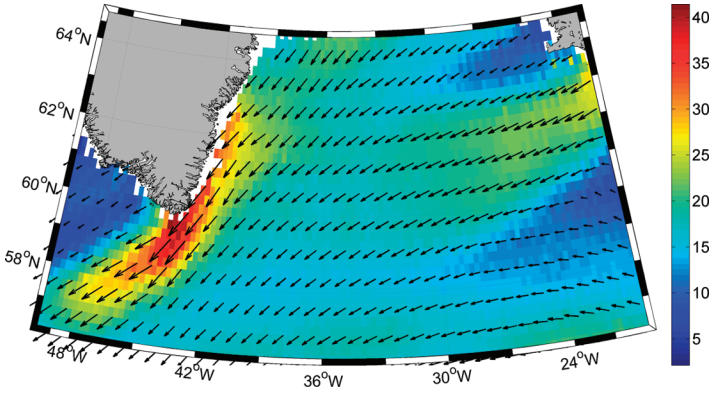

Fig. 3. QuikSCAT-derived 10-m winds for the morning of 21 Feb 2007 (the satellite passes are from 0718 and 0900 UTC). The colors show wind speed (m s^{-1}). The vectors are every third pixel (i.e., every 0.75°).

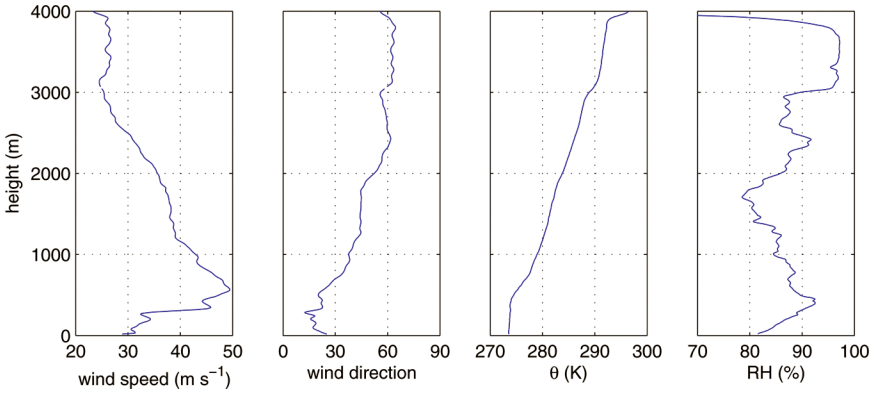

Fig 4. Profiles of wind speed, wind direction, potential temperature (θ), and RH from dropsonde 9 (60°N, 43°W) released at 1312 UTC 21 Feb 2007 during the reverse-tip jet flight.

dropsonde sections clearly show a low-level jet with the strongest winds at the coast and an acceleration downwind (not shown). Figure 4 shows atmospheric profiles from the dropsonde closest to the coast on the southernmost dropsonde section. There is a sharp jet in the winds with a maximum of 49 m s^{-1} about 600 m above sea level. The north-northeast jet is sharply defined up to about 1200 m, above which there is a slower dropoff in wind speed to ~3,000 m, above which wind speeds are approximately constant and from the east-northeast. The atmosphere is (nearly) neutral in stability from the surface up to about 500 m, and weakly stable above this, and is not particularly cold; the ABL potential temperature is 274 K. At this location the relative humidity (RH) is not particularly high, compared to the other dropsondes, consistent with there being less cloud visible at the coast in Fig 2. At flight level (not shown) we observed winds increasing from 25 to almost 35 m s^{-1} over the 70-km legs and an ABL that was undoubtedly turbulent. From our bird's-eye view we could see a sea that was raging: strong winds were ripping the tops of the waves off and hurling them downwind. Halfway through the low-level legs, when we turned into the jet and headed upwind, flying across the 5–10-m waves felt more like being on a rollercoaster, you could literally feel the ocean's swell. The first flight of the GFDex campaign was a great success; providing the first-ever in situ observations of these ferocious Greenland tip jets.

A polar mesoscale cyclone. On 25 February a mesoscale cyclone was situated to the north of Iceland near the island of Jan Mayen. This weather system had developed out of the remnants of a large-scale cyclone that had propagated northward along the coast of Norway over the preceding few days. The mesoscale system was forecast to intensify and move within range of the aircraft on 25 February. Flight B271 was planned to sample the three-dimensional structure of its wind and mass field through two perpendicular

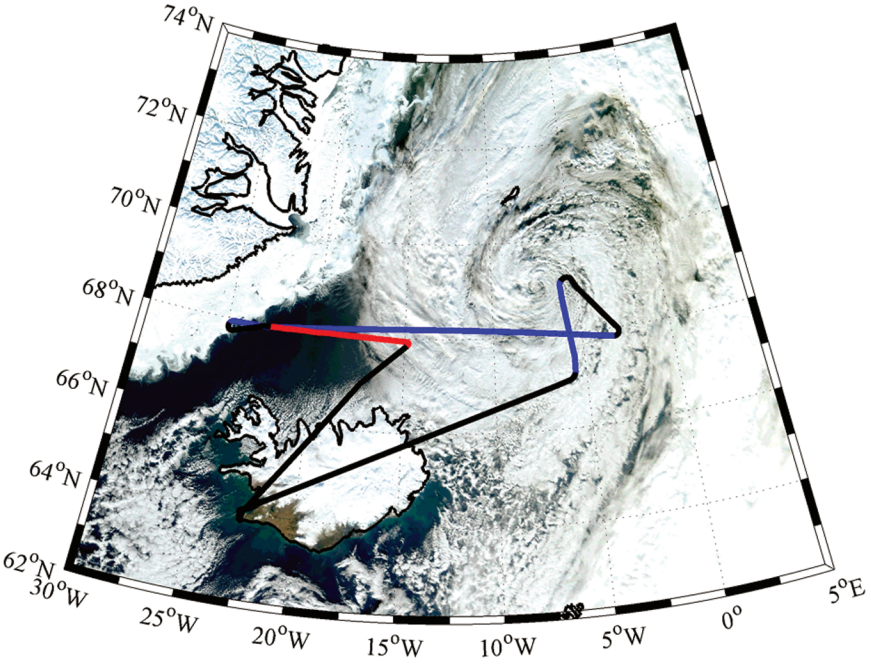

Fig. 5. MODIS true-color image from 1315 UTC 25 Feb 2007 showing the mesoscale cyclone that was the subject of flight B271. The flight track for this flight is shown with the black segments representing ferry or repositioning legs, the blue segments representing the high-level dropsonde legs (~7,600 m), and the red segment representing the low-level (~30 m) leg. The island of Jan Mayen can be seen to the north of the cyclone center. Sea ice flanking the coast of Greenland can be seen in the image, as can the snow cover over much of Iceland.

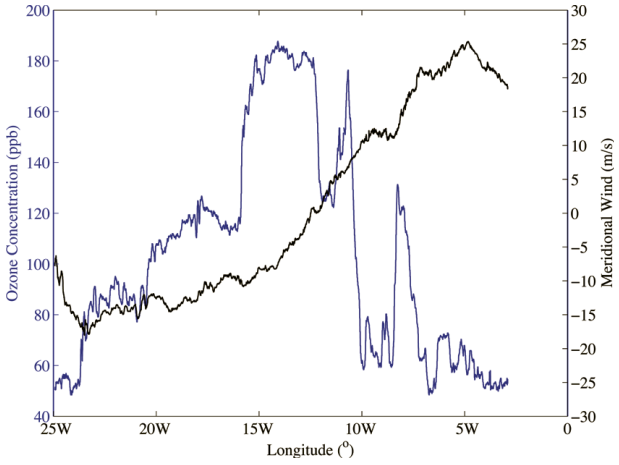

Fig. 6. Ozone concentration (blue) and the meridional component of the wind (black) from the flight-level data during the high-level east–west leg of flight B271.

dropsonde legs through the center of the circulation, as well as to fly a low-level leg close to the Greenland coast to investigate the impact that its topography had on the system's wind field. Figure 5 shows a visible image at the flight time; one can see that the cloud field has a number of filamentary features, as well as a central eye that is reminiscent of some of the more striking polar lows that have been studied over the past 20 yr (Rasmussen and Turner 2003). Indeed, during the flight a number of these cloud-free curved features, interspersed with deep convective cloud elements, were observed. The mesoscale cyclone's track differed from that forecast and, as a result, the mission did not pass precisely through the center of its circulation (Fig. 5). Figure 6 shows the meridional component of the wind and the ozone concentration along the high-level (~7,600 m) east–west leg. There is a reversal in the sense of the wind from southerly on the storm's eastern flank to northerly along its western flank. In the center of the circulation (defined by a meridional component of the wind close to zero) one can see a region of elevated ozone concentration (~180 ppb), most likely associated with a depression in the height of the tropopause. There is a number of other, narrower, regions of high ozone concentration that suggest a filamentary upper-level circulation similar to those associated with stratospheric intrusions (e.g., Appenzeller et al. 1996); a notion also supported by low temperature and dewpoint depression values on this leg (not shown). It is possible that this upper-level circulation (equivalent to an upper-level potential vorticity anomaly) was responsible for the development of the mesoscale cyclone (e.g., see Hoskins et al. 1985).

Dropsonde data along this leg (not shown) indicate that the low-level wind speeds on the system's western flank were as high as 25 m s^{-1}. Figure 7 shows the topography in the vicinity of the flight's low-level leg and the observed wind speed along this leg. At 22°W the wind speeds were low, rising to a narrow jet-like peak with wind speeds in excess of 15 m s^{-1} near 20°30′W, before a more general increase toward the center of the mesoscale cyclone. The wind direction was from the north. A comparison with the upstream topography indicates that the jet-like feature was situated downwind of a headland known as Liverpool Land (Fig. 7). It is possible that this feature was the result of barrier flow that occurred through an interaction of the northerly flow associated with the system and the topography of Greenland. At ~100 km offshore from the mountains the jet is within the Rossby radius of deformation for barrier flows of $R_R = V_g(f\mathrm{F_r})^{-1}$, where V_g is the geostrophic wind (~10 m s^{-1}), f is the Coriolis parameter (~1.2 x 10^{-4} s^{-1}), and Fr is the Froude number (estimated from the dropsondes to be ~0.7), giving values of $R_R \approx 120$ km (see Moore and Renfrew 2005).

The issue arises as to whether or not this system meets the definition of a "polar low." According to the so-called Paris definition (Rasmussen and Turner 2003), a polar low is a small, that is, less that 1,000 km in diameter, but intense, that is, with surface winds at gale force or above, maritime weather system that forms north of the main baroclinic zone. It is clear from the above description that this system meets this

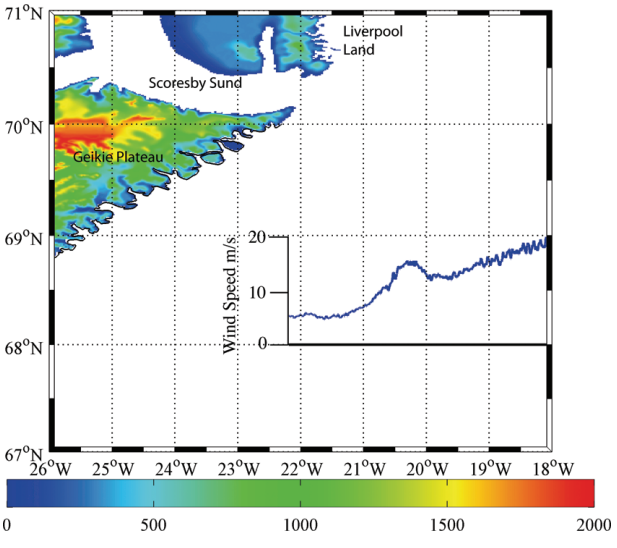

Fig. 7. Topography of southeast Greenland (shaded, m) in the vicinity of the low-level leg of flight B271. The flight track is shown as the thick black line along 68°N, while an inset shows the wind speed (m s^{-1}) along this leg.

definition. Because this is the case, flight B271 represents only the third time that in situ measurements have been made into a polar low. As such, the extended analysis of this system will undoubtedly provide further insight into this important class of high-latitude weather systems.

Barrier winds. On 1 and 2 March 2007 a sustained period of barrier winds developed off the southeast coast of Greenland. Initially, this barrier flow appeared coincident with a 975-hPa low pressure system to the north of Iceland, which was channeling flow from the north toward the Denmark Strait (Fig. 8a). A mesoscale cyclone just west of Iceland acted to extend this channeling effect to the south of the Denmark Strait. By 2 March, a synoptic-scale cyclone to the south had moved into the Irminger Sea region and deepened to 977 hPa, increasing the pressure gradient at the southeastern coast of Greenland and thus increasing the along-barrier winds that would be expected here (Fig. 8b). These 2 days provided a fantastic opportunity to observe the barrier flow over an evolving synoptic situation. Two flights were planned on consecutive days during which the same two high-level dropsonde legs could be flown to provide spatial and temporal evolutions of the barrier flow (B273 and B274; see Fig. 1 and Table 1). On the following day (3 March) a lee cyclone that developed off southeast Greenland (at 61°N, 37°W; see Fig. 8c) was targeted, and this is discussed in the next section.

Figure 9 shows a cross section of wind speed and wind direction from the second flight's northernmost cross section (see Fig. 8b for location). Observations from the dropsondes clearly show a jet in wind speed from around 60° from the north, confined to below the coastal mountain height. There is a jet maximum of about 25 m s^{-1} between 500 and 1,000 m above sea level, capped by a region of low wind speed extending up to 3,000 m, which is approximately the summit height of Greenland, before the wind speed increases again in the unobstructed southwesterly upper-level flow. It is interesting to note that the barrier jet maximum is some 100 km off the coast at this time. There is a large shear in wind direction between 2,500 and 3,000 m. Close to Greenland (between 0 and 100 km) the winds back smoothly round west-southwest, whereas farther off the coast (150–250 km) the winds veer round to the west-southwest. However, the winds at this height are rather light (~4 m s^{-1}); it is a col between two lows (similar to Fig. 8b), and so it is unlikely that this difference in directional shear is significant.

Low-level legs flying ~30 m above the sea were flown during the second flight (B274). Figure 10 show surface turbulent heat fluxes during a short leg (heading 320°) across the barrier flow. The heat fluxes are estimated using a well-established bulk flux algorithm based on Smith (1988; see also Renfrew et al. 2002). Wind speeds of approximately 20 m s^{-1}, combined with the cold air (~265 K) coming form the northeast, lead to surface sensible and latent heat fluxes of about 300 and 200 W m^{-2}, respectively. This combined surface turbulent heat flux of over 500 W m^{-2}, which is more than the incoming clear-sky solar radiation at

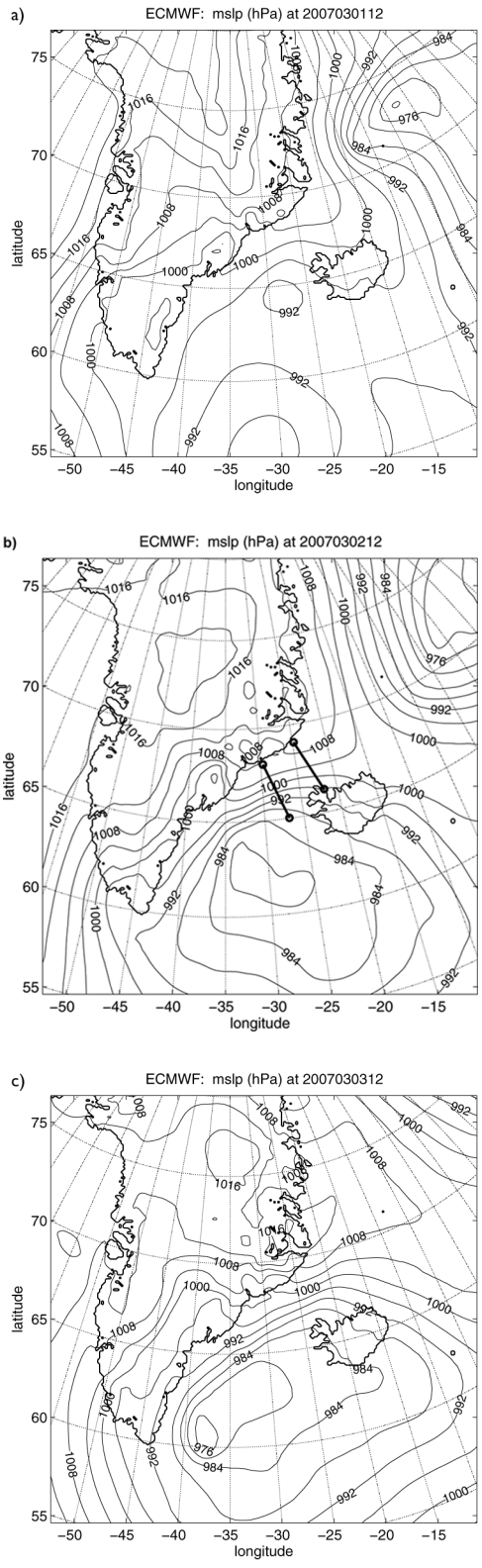

Fig. 8. ECMWF analyses of mean sea level pressure at 1200 UTC (a) 1 Mar, (b) 2 Mar, and (c) 3 Mar 2007. Isobars are every 4 hPa. (b) The location of the barrier flow dropsonde legs flown during B273 and B274 are overlaid.

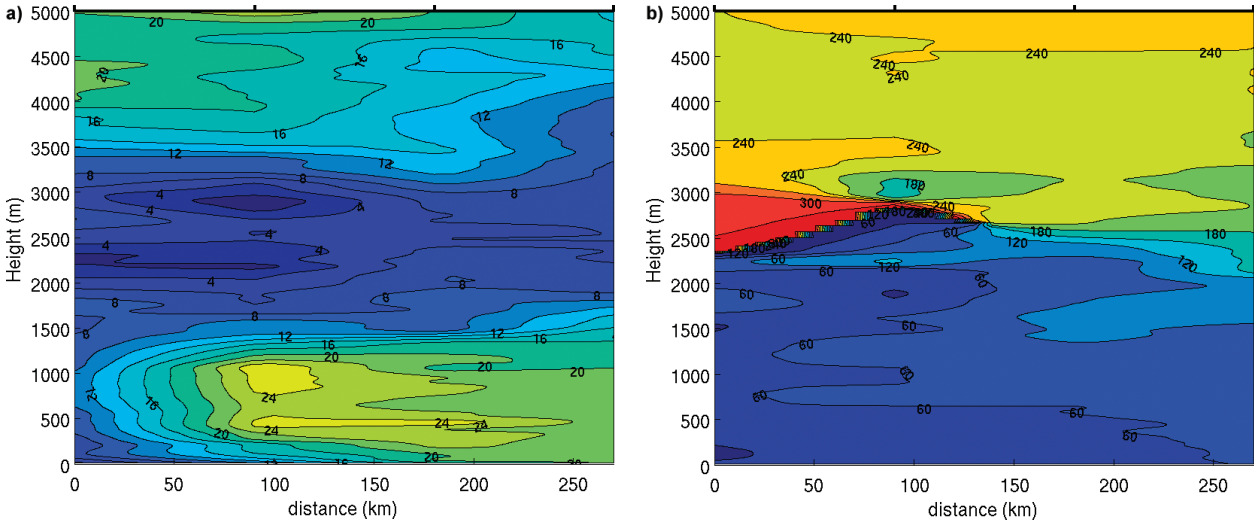

Fig. 9. Observed cross sections of (left) wind speed and (right) wind direction at ~1245 UTC 2 Mar 2007, as derived from soundings from the northernmost dropsonde leg of B274. Contours are every 2 m s^{-1} and every 30°. The sections run from northeast to southwest.

this location, is of a sufficient magnitude to have a significant impact on the ocean. For example, one diagnostic that indicates the impact on the ocean is the buoyancy flux, the rate at which the surface layers are gaining or losing density (e.g., Marshall and Scott 1999). For this event, the buoyancy flux was approximately -2×10^{-7} m^2 s^{-3}, which is larger than the values quoted for open-ocean convective events in the Labrador and Greenland Seas by Marshall and Schott (1999). Furthermore, if sustained over 24 h, this heat flux would lead to a sea surface temperature drop of 0.22 K (based on a mixed layer of 50 m, an estimate taken from the nearest available Argo float at this time), which is a significant decrease.

A lee cyclone. Over 50 yr ago, Petterssen (1956) showed that the region off of Greenland's southeast coast has a higher frequency of low centers than almost any other region on Earth. Subsequent model studies have indicated that Greenland's orography causes lee cyclone formation in this area during westerly flow over Greenland (Kristjánsson and McInnes 1999; Petersen et al. 2003; Skeie et al. 2006), but the details of this process are not well known. On 3 March 2007 such a lee cyclogenesis event was, for the first time, explored with in situ aircraft measurements.

The weather conditions during the week preceding this event were dominated by a blocking pattern with generally rather weak easterly winds over southern Greenland at 500 hPa. This changed dramatically from 28 February 2007 onward, as a surge of Arctic air swept over Greenland in the rear of a deepening upper-level low moving southeast over Jan Mayen. Figure 8a shows the surface mean sea level pressure feature associated with this low on 1 March 2007. The NWP forecast models all indicated dramatic lee cyclogenesis over the next couple of days, but there was disagreement about the strength and position of the cyclogenesis.

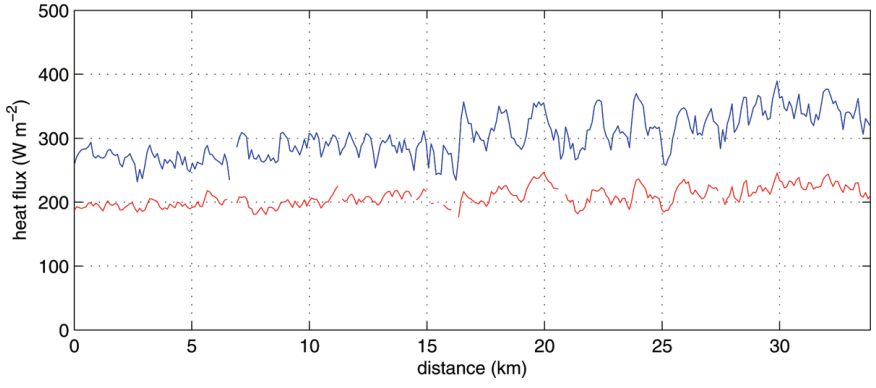

Fig. 10. Surface sensible (blue) and latent (red) heat fluxes between 1327 and 1332 UTC 2 Mar 2007 from a 40-m altitude leg during flight B274. The leg is underneath the northernmost dropsonde leg shown in Figs. 8b and 9.

In order to capture the developing phase of the cyclone, part of the 1 March flight (B273; see Fig. 1 and Table 1) released dropsondes into the "precursor low" around 64°N, 37°W. At

this stage the weather in that area was fairly quiet, with scattered snow showers. On 2 March the preconditioning phase continued with the following three identifiable causal factors: i) orographic vortex stretching; ii) a gradually increasing northeasterly cold-air outflow off Greenland's east coast, that is, the barrier winds summarized above and their associated strong heat fluxes (Figs. 8b and 10); and iii) a broad cyclone to the south, moving slowly northward, advecting warm air toward the region of interest (Fig. 8b).

The most rapid development phase of the cyclone was from 1200 UTC 2 March to 1200 UTC 3 March 2007 (Figs. 8b,c), with the latter time coinciding with flight B275. Figure 11 shows the B275 flight track overlaid on an AVHRR visible satellite image. The mission took off to the west-southwest with a plan to cross the surface low center from the northeast to southwest, before heading north on the west side of the low, and crossing the center again from the northwest to southeast, all at 7,500 m and dropping sondes. This was to be followed by three shorter 1,500-m legs, mapping out the frontal structure of the low. The position of the low center was forecast to be at 61°N, 38°W. As it turned out, the center of the low was somewhat farther southeast than any of the models had indicated, meaning that the last two legs had to be redesigned in flight. To complicate matters further, the low was moving south-southeast during the flight. In order to obtain flight-level data right in "the eye," it was finally decided to simply fly perpendicular to the flight-level wind at 1,500 m, with the wind hitting the aircraft on its left side.

As the satellite image shows, this was a mature cyclone with a bent-back occlusion wrapping around the low center. The air was extremely dry near the cyclone center, with a dewpoint depression of 9 K at 800 hPa, rising to 25 K at 750 hPa, suggesting a possible stratospheric intrusion; this notion was corroborated by unusually high ozone measurements (~150 ppb near the low center rising to ~230 ppb to the west of it, both at ~7,500 m). Behind the frontal systems, to the east side of the low, there were widespread cumulonimbus and cumulus clouds with showers (Fig. 11). Another conspicuous feature in Fig. 11 is the dark area from 62°N, 32°W to about 60°N, 25.5°W. Why is this fairly large area, close to the center, virtually cloud free? Analyzing the surface pressure measured in our first dropsondes in leg 1, we find strong evidence of a second low center located near 62°N, 32°W, and it seems possible that the lack of clouds here is due to subsidence, somewhat similar to that found near the main low center. Earlier model simulations (e.g., Petersen et al. 2004) have indicated a tendency for lows moving in this region to be shifted toward Greenland because of orographic forcing. In line with those findings, one may conceivably interpret the double-low structure as being caused by a combination of orographic forcing, tending to pull the low toward Greenland, competing with dynamical (e.g., upper level) forcing, tending to create a low farther east.

The dropsonde data, as well as the low-level data, revealed very distinct mesoscale features, for example, a central "eye" and a surrounding "eyewall" (to borrow terminology from tropical cyclones). Flying through the northern edge of the low center early in the flight, the eye was quite distinct because the dense cloud deck suddenly disappeared and we saw a tranquil sea surface underneath us for a few minutes. Ahead of us, toward the west, we saw a wall of cumulonimbus clouds, reaching almost up to the level of

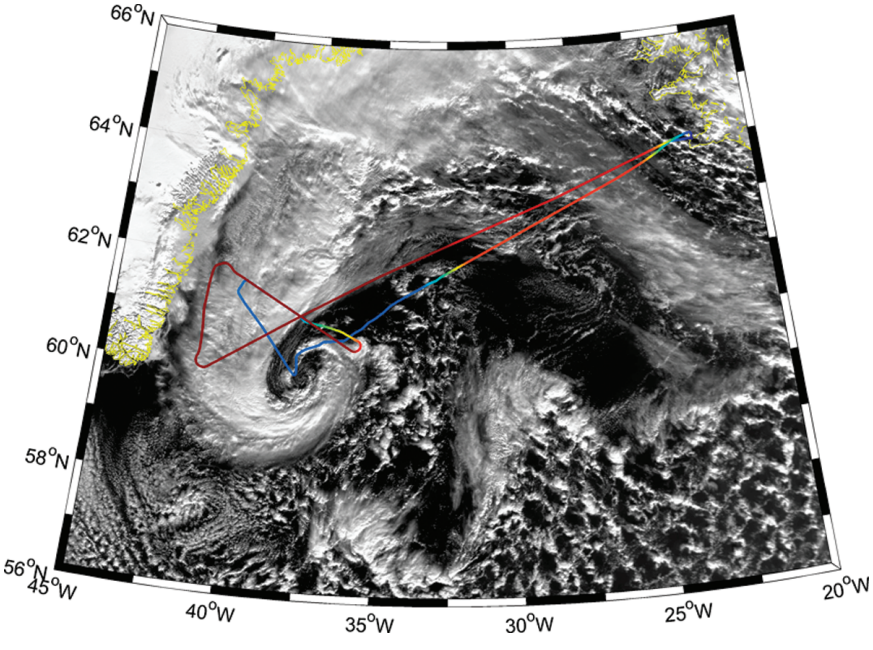

Fig. 11. Lee cyclone flight track (B275) overlaid on a visible (channel 1) AVHRR satellite image from 1343 UTC 3 Mar 2007. The colors in the flight track indicate the aircraft's altitude from low (blue, ~1,500 m) to high levels (red, ~7,500 m).

the aircraft (7,500 m). The development of such deep cumulonimbus clouds would be augmented by the very strong air–sea heat fluxes at this time (Fig. 10). During the 1,500-m legs through the frontal systems conditions were quite rough, especially in the "cloud wall" west of the low center where we experienced wind speeds of 20–30 m s^{-1}, temperatures between –10° and –15°C, heavy snowfall, and snow accumulation on the aircraft.

THE TARGETED OBSERVATIONS PROGRAM. The aim of targeted observations is to improve NWP forecasts for a predefined region (the *verification region*) by adding observational data (e.g., from dropsondes) into the initial conditions of the forecast. The question then is where to target these additional observations? To answer this, so-called Sensitive Area Predictions (SAPs) are made; these theoretically maximize the forecast improvement in the verification region by reducing errors in the initial conditions. Figure 12 illustrates the timelines involved. The time between initializing the forecasts used to make the SAP and making the additional observations (the *targeting time*) is termed the *lead time*; the time between targeting and forecast verification is termed the *optimization time*. The optimization time needs to be short enough for the SAP calculations to be valid, but long enough to allow flow perturbations to propagate from the sensitive region into the verification region.

Sensitive area prediction methods. During GFDex two techniques were used to identify the target region—singular vectors (SVs) and the ensemble transform Kalman filter. Singular vectors are used to identify regions where the forecast is sensitive to small, rapidly growing errors in the initial conditions. They are constrained to identify the fastest-growing perturbations, impacting the verification region, with respect to a defined norm. Total energy has been shown to be an appropriate norm for targeting (Buizza and Palmer 1995), although other norms have also been used. The dominant SVs are typically located in areas of cyclogenesis. Only the 5–10 fastest-growing SVs need to be identified and vertically averaged to get an accurate representation of the sensitive area (Buizza and Palmer 1995).

The ensemble transform Kalman filter (ETKF) is used to identify regions where the analysis error is large. It uses a test set of targeted observations and determines where these should be placed within a routine observing network to get the maximum reduction in forecast error in the verification region (Bishop et al. 2001; Majumdar et al. 2002). Singular vectors identify the locations of the fastest-growing errors for a given time period. Therefore, they will identify regions of the forecast where the errors are initially small and amplify rapidly, but not regions where the errors are already large at the time the forecast is initialized. In contrast, the ETKF identifies locations where errors lead to large errors at the analysis time and so will identify both of these regions. In addition, the ETKF includes a coarse approximation to the routine observing network and so will not give SAPs where there is dense coverage by conventional observations; conversely, the SV technique does not take into account routine observations and thus may identify areas with a dense observing network, such as over the United Kingdom. The different characteristics of SVs and the ETKF mean that the sensitive areas they identify often differ. Leutbecher et al. (2004) showed that for the period of the Atlantic THORPEX Regional Campaign (ATReC) the sensitive areas calculated by the different methods overlapped by more than 0.5 only 46% of the time. However, this lack of overlap does not mean that one method has correctly identified a region of forecast sensitivity and one has not.

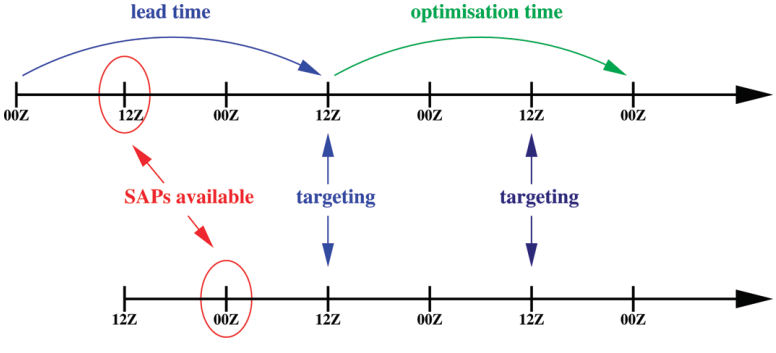

FIG. 12. A schematic of the timeline involved in the targeted observation program. Forecast initialization is at (top) 0000 and (bottom) 1200 UTC with verification times 72 and 60 h later, respectively. The time between forecast initialization and targeting is termed the lead time. The forecasts initialized at 0000 (1200) UTC produce SAPs with 36 and 60 h (24 and 48 h) lead times. The time between targeting and forecast verification is termed the optimization time, illustrated here at 36 h.

Sensitive area predictions for GFDex. SAPs were provided for GFDex by the ECMWF and Met Office. ECMWF provided predictions based on total energy singular vector

(TESV) calculations at T42 truncation and 62 vertical levels, run on output from the ECMWF deterministic forecast, which was running with a T799 truncation and 91 vertical levels (a model top at 0.1 hPa). TESVs are calculated operationally at ECMWF to determine the perturbations for their ensemble prediction system. The Met Office provided predictions based on the ETKF run on output with 2.5° grid spacing from the Met Office Global and Regional Ensemble Prediction System (MOGREPS), which is a 24-member ensemble designed for shorter-range forecasts over a limited North Atlantic–European domain (see Bowler et al. 2006).

Two fixed verification regions were prescribed: northwest Europe (centered on the United Kingdom; see Fig. 13) and Scandinavia (54°–74°N, 0°–40°E). Each region is approximately 2,000 km^2, which is similar in size to previous targeting campaigns (e.g., Montani et al. 1999; Petersen and Thorpe 2007). SAPs were provided with four lead times (24, 36, 48, and 60 h) and three optimisization times (24, 36, and 48 h). From initialization time it took 7–8 h for the SV SAPs and 10–11 h for the ETKF SAPs to be received. The nominal targeting time was fixed at 1200 UTC, although in practice targeting was performed over a window of ~4 h, typically from 0930 to 1330 UTC so as to enable the observations to be assimilated into operational 1200 UTC forecasts. The dropsonde data were transmitted from the aircraft onto the GTS via a satellite communication link.

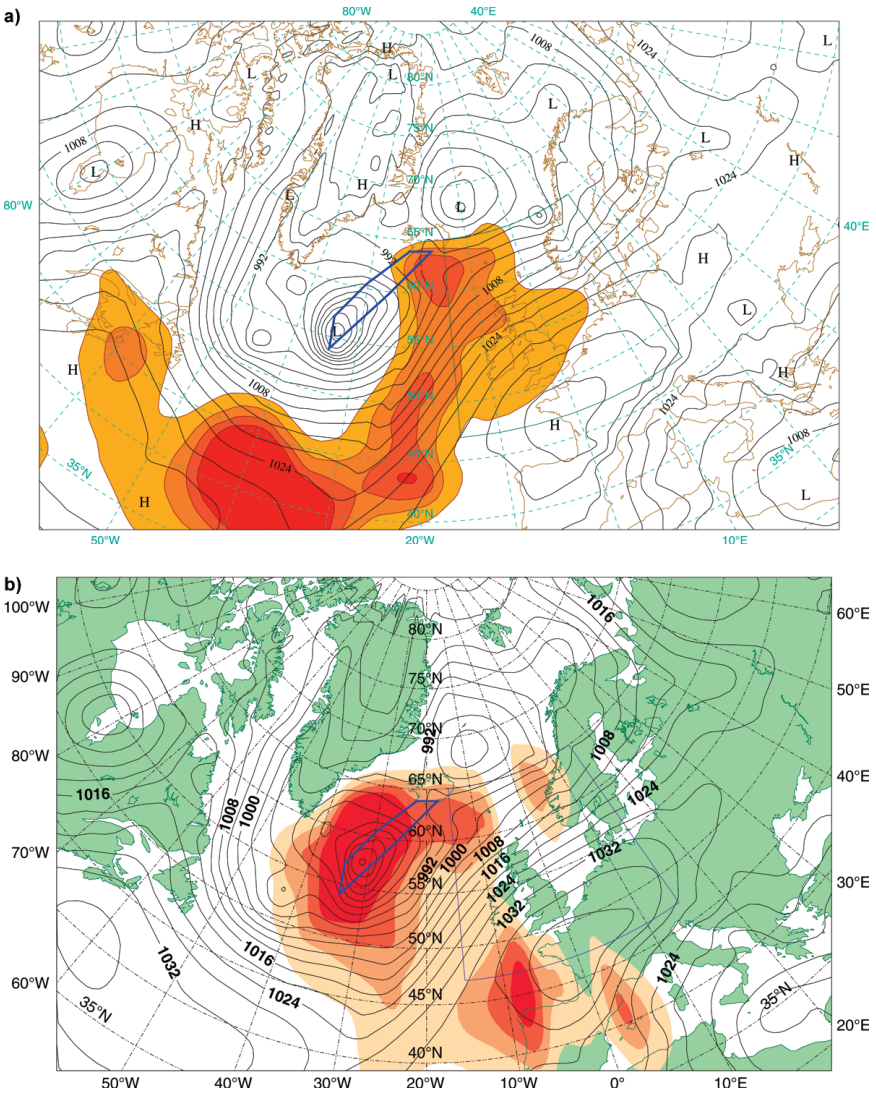

Fig. 13. Targeting guidance for 1200 UTC 10 Mar 2007 for a lead time of 36 h and optimization time of 48 h: SAP plots of (top) SVs from the ECMWF and (bottom) ETKF from the Met Office both for the northwest Europe verification region. The most sensitive 1, 2, 4, and 8 x 10^6 km^2 of the forecast are shaded. The black contours are mean sea level pressure at the targeting time (contour interval 4 hPa) and the green (top) and blue (bottom) boxes show the verification regions. The flight track for B279 is shown in bold.

A targeted observation case. A targeted observation mission was undertaken on 10 March 2007 as part of flight B279. The primary aim of the flight was to improve the 24-, 36-, and 48-h forecasts over northwest Europe and Scandinavia by making additional observations in a synoptic-scale cyclone located southwest of Iceland. The ETKF SAPs were used as targeting guidance for flight planning. These identified the center of the low pressure system as being highly sensitive for both verification regions; in contrast, the TESV SAPs identified the outer edge on the eastern side of the low pressure system as sensitive. Figure 13 show SAPS for the northwest Europe verification region. The SAPs are similar for the Scandinavian region. Note the ETKF had above-average maximum signal variances

in the SAP area, compared to other SAPs from the campaign period. Note the flight had the following two further aims: to map out the structure of the developing synoptic-scale cyclone and to capture breaking gravity waves over Hvannadalshnjukur, a mountain in southeast Iceland.

The synoptic-scale cyclone that was targeted developed off the eastern U.S. seaboard. During the 24 h preceding targeting, it moved rapidly across the North Atlantic, deepening by 38 hPa. At the time of targeting the cyclone was baroclinic in structure, becoming more barotropic as it began to decay and move slowly eastward across Iceland, battering the GFDex detachment with strong winds and heavy rain.

The flight was planned with the first dropsonde leg passing to the west of the cyclone center and the return leg passing to the east. However, the cyclone was located farther west than forecast, which resulted in the first dropsonde leg flying through the center of the cyclone. Nine targeted dropsondes were released, with an additional five dropsondes released to help realize the additional aims of the flight. All soundings were assimilated into the 1200 UTC forecast at the Met Office, and were available via the Global Telecommunication System (GTS) to all forecasting centers. The targeted observations revealed that the strength of the cyclone had been underpredicted by 12–16 hPa by the 36-h Met Office and ECMWF forecasts. The impact of the targeted observations on the forecast downstream of the target region is currently being assessed through hindcast studies. It is hoped that the targeted observations will have corrected the background field used to initialize the model, and thus improve the forecast over Europe and Scandinavia.

CONCLUSIONS AND FUTURE WORK. The Greenland Flow Distortion Experiment has provided a number of observational first looks at the strong winds and intense mesoscale weather systems that occur around the coastal seas of Greenland and Iceland. Detailed analysis of the aircraft-based observations is underway, as is a comprehensive numerical modeling program using a suite of models [including the Unified Model (UM), MM5, and Weather Research and Forecasting (WRF)]. A number of detailed "case study" papers are anticipated, focusing on the structure, dynamics, and associated air–sea interactions of the weather systems highlighted here, for example, the reverse tip jet, the Jan Mayen polar low, the lee cyclone event, and the barrier wind cases. In addition, all of the low-level turbulence observations are being worked up into covariance fluxes of heat, moisture, and momentum, providing rare aircraft-based turbulent fluxes in high wind speed open-ocean conditions, and complimenting the few similar ship-based datasets available. The aircraft and dropsonde data are also being used to assess the quality of a number of satellite products (e.g., QuikSCAT winds) and meteorological analyses. The impact of the targeted observations is currently being assessed through hindcast studies, in collaboration with the Met Office. In conclusion, we anticipate that GFDex will enable a dramatic improvement in our meteorological understanding in this area and its role in atmospheric predictability and the climate system.

ACKNOWLEDGMENTS. The GFDex would not have been possible without the dedication and flexibility shown by all at the FAAM, DirectFlight, and Avalon. GFDex was funded by the Natural Environmental Research Council (NE/C003365/1), the Canadian Foundation for Climate and Atmospheric Sciences (GR-641), and the European Union Fleet for Airborne Research (EUFAR) and European Union Coordinated Observing System (EUCOS) schemes. In particular, we would like to thank the managers and facilitators of these two EU schemes: John Foot, Dave Kindred, Jim Caughey, Stuart Goldstraw, Stefan Klink, Rudolf Krockauer, Hreinn Hjartarson, and Nis Jepsen. We would like to acknowledge the role of the International Polar Year in providing contacts and an embryonic IPY THORPEX research network. The experiment received real-time data support from the Dundee Satellite Receiving Station, the Met Office, the Vedurstofa Islands (Icelandic Meteorological Office), the ECMWF, and the Storm Weather Centre (Norway); we would like to thank Neil Lonie, Andrew Brooks, Tim Hewson, and Sæunn Halldórsdóttir for their contributions here. We would like to acknowledge help from the Icelandic Aviation Authorities during the field program and the British Atmospheric Data Centre, particularly Wendy Garland, for archiving the GFDex data (see http://badc.nerc.ac.uk./data/gfdex/). Finally, we would like to thank the paper reviewers for their thoughtful suggestions.

REFERENCES

Appenzeller, C., H. C. Davies, and W. A. Norton, 1996: Fragmentation of stratospheric intrusions. *J. Geophys. Res.*, **101,** 1435–1456.

Bacon, S., G. Reverdin, I. G. Rigor, and H. M. Smith, 2002: A freshwater jet on the east Greenland shelf. *J. Geophs. Res.*, **107,** 3068, doi:10.1029/2001JC000935.

Bishop, C. H., B. J. Etherton, and S. J. Majumdar, 2001: Adaptive sampling with the ensemble transform Kalman filter. Part I: Theoretical aspects. *Mon. Wea. Rev.*, **129,** 420–436.

Bowler, N. E., A. Arribas, K. R. Mylne, and K. B. Robertson, 2006: Met Office Global and Regional Ensemble Prediction system (MOGREPS) Part I: System description. Met Office Tech. Rep. 497, 21 pp.

Buizza, R, and T. N. Palmer, 1995: The singular-vector structure of the atmospheric global circulation. *J. Atmos. Sci.*, **52,** 1434–1456.

Cappelen, J., B. V. Jorgensen, E. V. Laursen, L. S. Stannius, and R. S. Thomsen, 2001: The observed climate of Greenland, 1958–1999, with climatological standard normals, 1961–1990. Danish Meteorological Institute Tech. Rep. 00-18, 149 pp.

Condron, A., G. R. Bigg, and I. A. Renfrew 2006: Polar mesoscale cyclones in the northeast Atlantic: Comparing climatologies from ERA-40 and satellite imagery. *Mon. Wea. Rev.,* **134,** 1518–1533.

——, ——, and ——, 2008: Modeling the impact of polar mesocyclones on ocean circulations. *J. Geophys. Res.*, in press.

Doyle, J. D., and M. A. Shapiro, 1999: Flow response to large-scale topography: The Greenland tip jet. *Tellus*, **51A,** 728–748.

——, ——, Q. Jiang, and D. L. Bartels, 2005: Large-amplitude mountain wave breaking over Greenland. *J. Atmos. Sci.*, **62,** 3106–3126.

Egger, J. 2006: Winter time flow over and around Greenland: Trajectories related to torques. *Tellus*, **58A,** 584–592.

Fehsenfeld, F. C. and Coauthors, 2006: International Consortium for Atmospheric Research on Transport and Transformation (ICARTT): North America to Europe—Overview of the 2004 summer field study. *J. Geophys. Res.*, **111,** D23S01, doi:10.1029/2006JD007829.

Haine, T., 2008: What did the Viking discoverers of North America know of the North Atlantic environment. *Weather*, **63,** 60–65.

Harold, J. M., G. R. Bigg, and J. Turner, 1999: Mesocyclone activity over the north-east Atlantic. Part I: Vortex distribution and variability. *Int. J. Climatol.*, **19,** 1187–1204.

Heinemann, G., 1999: The KABEG '97 field experiment: An aircraft-based study of katabatic wind dynamics over the Greenland ice sheet. *Bound.-Layer Meteor.*, **93,** 75–116.

Hoskins, B. J., M. E. McIntyre, and A. W. Robertson, 1985: On the use and significance of isentropic potential vorticity maps. *Quart. J. Roy. Meteor. Soc.*, **111,** 877–946.

Klein, T., and G. Heinemann, 2002: Interaction of katabatic winds and mesocyclones near the eastern coast of Greenland. *Meteor. Appl.*, **9,** 407–422.

Kristjánsson, J. E., and H. McInnes, 1999: The impact of Greenland on cyclone evolution in the North Atlantic. *Quart. J. Roy. Meteor. Soc.*, **125,** 2819–2834.

Langland, R. H., and Coauthors, 1999: The North Pacific Experiment (NORPEX-98): Targeted observations for improved North American weather forecasts. *Bull. Amer. Meteor.*, **80,** 1363–1384.

Lavender, K. L., R. E. Davis, and W. B. Owens, 2000: Mid-depth recirculation observed in the interior Labrador and Irminger seas by direct velocity measurements. *Nature,* **407,** 66–69.

Leutbecher, M., J. Barkmeier, T. N. Palmer, and A. J. Thorpe, 2002: Potential improvement to forecasts of two severe storms using targeted observations. *Quart. J. Roy. Meteor. Soc.*, **128,** 1641–1670.

——, A. Doerenbecher, F. Grazzini, C. Cardinali, 2004: Planning of adaptive observations during the Atlantic THORPEX Regional Campaign 2003. ECMWF Newsletter, Winter Issue 102, 16–25.

Majumdar, S. J., C. H. Bishop, and B. J. Etherton, 2002: Adaptive sampling with the Ensemble Transform Kalman Filter. Part II: Field program implementation. *Mon. Wea. Rev.*, **130,** 1356–1369.

Marshall, J., and F. Schott, 1999: Open-ocean convection: Observations, theory and models. *Rev. Geophys.,* **37,** 1–64.

Martin, R. ., and G. W. K. Moore, 2008: Air-sea interaction associated with a Greenland reverse tip jet. *Geophys. Res. Lett.,* **34,** L24802, doi:10.1029/2007GL031093.

Marwitz, J., M. Politovich, B. Bernstein, F. Ralph, P. Neiman, R. Ashenden, and J. Bresch, 1997: Meteorological conditions associated with the ATR72 aircraft accident near Roselawn, Indiana, on 31 October 1994. *Bull. Amer. Meteor. Soc.*, **78,** 41–52.

Montani, A., A. J. Thorpe, R. Buizza, and P. Unden, 1999: Forecast skill of the ECMWF model using targeted observations during FASTEX. *Quart. J. Roy. Meteor. Soc.*, **125,** 3219–3240.

Moore, G. W. K. 2003: Gale force winds over the Irminger Sea to the east of Cape Farewell, Greenland. *Geophys. Res. Lett.*, **30,** 1894, doi:10.1029/2003GL018012.

——, and I. A. Renfrew, 2005: Tip jets and barrier winds: A QuikSCAT climatology of high wind speed events around Greenland. *J. Climate*, **18,** 3713–3725

Ólafsson, H., 1998: Different predictions by two NWP models of the surface pressure field northeast of Iceland. *Meteor. Appl.*, **5,** 253–261.

——, and P. Bougeault, 1996: Nonlinear flow past an elliptic mountain ridge. *J. Atmos. Sci.*, **53,** 2465–2489.

——, and ——, 1997: The effect of rotation and surface friction on orographic drag. *J. Atmos. Sci.*, **54,** 193–210.

Orr, A., E. Hanna, J. C. R. Hunt, C. R. J. Cappelen, K. Steffen, and A. G. Stephens, 2005: Characteristics of stable flows over Southern Greenland. *Pure Appl. Geophys.*, **162,** 1747–1778.

Parish, T. R. 1982: Barrier winds along the Sierra-Nevada Mountains. *J. Appl. Meteor.*, **21,** 925–930.

——, 1983: The influence of the Antarctic Peninsula on the wind-field over the western Weddell Sea. *J. Geophys. Res.*, **88,** 2684–2692.

Petersen, G. N., and A. J. Thorpe, 2007: The impact on weather forecast of target observations during A-TReC. *Quart. J. Roy. Meteor. Soc.*, **133,** 417–431.

——, H. Ólafsson, and J. E. Kristjánsson, 2003: Flow in the lee of idealized mountains and Greenland. *J. Atmos. Sci.*, **60,** 2183–2195.

——, J. E. Kristjánsson, and H. Ólafsson, 2004: Numerical simulations of Greenland's impact on the Northern Hemispher winter circulation. *Tellus*, **56A,** 102–111.

——, ——, and ——, 2005: The effect of upstream wind direction on atmospheric flow in the vicinity of a large mountain. *Quart. J. Roy. Meteor. Soc.*, **131,** 1113–1128.

Petterssen, S., 1956: *Motion and Motion Systems.* Vol. 1. *Weather Analysis and Forecasting,* 2nd ed. McGraw Hill, 428 pp.

Pickart, R. S., M. A. Spall, M. H. Ribergaard, G. W. K. Moore, and R. F. Milliff, 2003: Deep convection in the Irminger Sea forced by the Greenland tip jet. *Nature*, **424,** 152–156.

——, K. Våge, G. W. K. Moore, I. A. Renfrew, M. H. Ribergaard, and H. C. Davies, 2008: Covection in the western North Atlantic subpolar gyre: Do small-scale wind events matter? *Arctic-Subarctic Ocean Fluxes*: *Defining the Role of the Northern Seas in Climate*, R. Dickson, Ed., Springer, 629–652.

Rasmussen, E. A., and J. Turner, 2003: *Polar Lows*: *Mesoscale Weather Systems in the Polar Regions*. Cambridge University Press, 612 pp.

Renfrew, I. A., G. W. K. Moore, T. D. Holt, S. W. Chang, and P. Guest, 1999: Mesoscale forecasting during a field program: Meteorological support of the Labrador Sea Deep Convection Experiment. *Bull. Amer. Meteor. Soc.,* **80,** 605–620.

——, ——, P. S. Guest, and K. Bumke, 2002: A comparison of surface-layer and surface turbulent-flux observations over the Labrador Sea with ECMWF analyses and NCEP reanalyses. *J. Phys. Oceanogr.*, **32,** 383–400.

Schwerdtfeger, W., 1975: Effect of Antarctic Peninsula on temperature regime of Weddell Sea. *Mon. Wea. Rev.*, **103,** 45–51.

Schwierz, C. B., and H. C. Davies, 2003: Evolution of a synoptic-scale vortex advecting toward a high mountain. *Tellus*, **55A,** 158–172.

Shapiro, M. A., and A. J. Thorpe, 2004: THORPEX International science plan. WWRP, WMO/TD-No. 1246, 57 pp. [Available online at www.wmo.int/pages/prog/arep/thorpex.]

——, H. Ólafsson, S. Low-Nam, J. D. Doyle, and P. Smolarkiewicz, 2002: Large-amplitude gravity-wave breaking over the Greenland lee and the subsequent formation of downstream, synoptic-scale, tropopause folding and stratospheric-tropospheric exchange. Preprints, 10th *Conf. on Mountain Meteorology,* Park City, UT. *Amer. Meteor. Soc.*, 5.1. [Available online at http://ams.confex.com/ams/pdfpapers/39939.pdf.]

Skeie, R. B., J. E. Kristjánsson, H. Ólafsson, and B. Røsting, 2006: Dynamical processes related to cyclone development near Greenland. *Meteor. Z.*, **15,** 147–156.

Smith, S. D., 1988: Coefficients for sea surface wind stress, heat flux, and wind profiles as a function of wind speed and temperature. *J. Geophys. Res.*, **93,** 15 467–15 472.

Spall, M. A., and R. S. Pickart, 2003: Wind-driven recirculations and exchange in the Labrador and Irminger Seas. *J. Phys. Oceanogr.*, **33,** 1829–1845.

Sproson, D. A. J., I. A. Renfrew, and K. J. Heywood, 2008: Atmospheric conditions associated with oceanic convection in the south-east Labrador Sea, *Geophys. Res. Lett.,* **35,** L06601, doi:10.1029/2007GL032971.

Stringer, S., and B. Truscott, 2004: Atlantic-THORPEX Regional Campaign: Operations manual. EUCOS/SP/106. [Available online at www.wmo.int/pages/prog/arep/thorpex/.]

Szunyogh, I., Z. Toth, R. E. Morss, S. J. Majumdar, B. J. Etherton, and C. H. Bishop, 2000: The effect of targeted dropsonde observations during the 1999 Winter Storm Reconnaissance Program. *Mon. Wea. Rev.*, **128,** 3520–3537.

Våge, K., R. S. Pickart, G. W. K. Moore, and M. H. Ribergaard, 2008: Winter mixed-layer development in the central Irminger Sea: The effect of strong, intermittent wind events. *J. Phys. Oceanogr.*, **38,** 541–565.

van den Broeke, M. R., and H. Gallee, 1996: Observations and simulation of barrier winds at the western margin of the Greenland ice sheet. *Quart. J. Roy. Meteor. Soc.*, **122,** 1365–1383.

Weissmann, M., R. Busen, A. Dornbrack, S. Rahm, and O. Reitebuch, 2005: Targeted observations with an airborne wind lidar. *J. Atmos. Oceanic Technol.*, **22,** 1706–1719.